# Graphene Plasmonics for Terahertz to Mid-Infrared Applications

**Tony Low*** **and Phaedon Avouris***

IBM T.J. Watson Research Center, 1101 Kitchawan Road, Yorktown Heights, New York 10598, United States

**ABSTRACT** In recent years, we have seen a rapid progress in the field of graphene plasmonics, motivated by graphene's unique electrical and optical properties, tunability, long-lived collective excitation and its extreme light confinement. Here, we review the basic properties of graphene plasmons: their energy dispersion, localization and propagation, plasmon–phonon hybridization, lifetimes and damping pathways. The application space of graphene plasmonics lies in the technologically significant, but relatively unexploited terahertz to mid-infrared regime. We discuss emerging and potential applications, such as modulators, notch filters, polarizers, mid-infrared photodetectors, and mid-infrared vibrational spectroscopy, among many others.

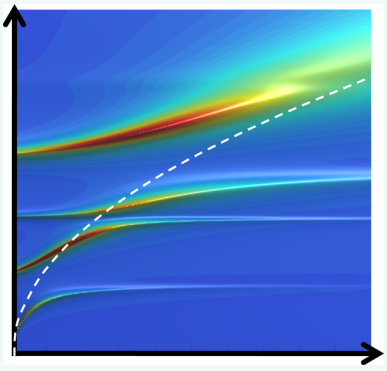

**KEYWORDS:** graphene plasmonics · terahertz · mid-infrared · damping · applications · metamaterials · spectroscopy · plasmonic devices · plasmon–polaritons · plasmon–phonon–polaritons

Plasmonics[1] is an important subfield of photonics that deals with the excitation, manipulation, and utilization of surface plasmon polaritons (SPP, hereafter also called simply plasmons), the quantum of elementary excitation involving the collective electron oscillation.[2] Over the past decade or so, research has focused mainly on noble metals plasmonics, with silver and gold being the predominant materials of choice. Today, metal plasmonics constitute the foundational pillars for applications as diverse as nanophotonics for integrated photonic systems,[3–5] metamaterials with unusual electromagnetic phenomena,[6–9] biosensing with nanostructures,[10,11] photovoltaic devices,[12] single photon transistors for quantum computing[13,14] and surface-enhanced Raman spectroscopy for single molecule detection.[15,16] These breakthroughs were realized in the visible to near-infrared frequencies.

In the ongoing search for new and better plasmonic materials,[17] graphene has emerged to be a very promising candidate for terahertz to mid-infrared applications,[18–23] the frequency range where its plasmonic resonance resides. Today, the terahertz to mid-infrared spectrum, which typically ranges from 10 to 4000 $cm^{-1}$, is finding a wide variety of applications[24–26] in information and communication, medical sciences, homeland security, military, chemical and biological sensing, and spectroscopy, among many others. In this review, we describe the recent advances made in the basic understanding and engineering of plasmons in graphene metamaterials, and provide our perspective on their potential application space.

**Graphene as a Tunable Optical Material.** Accompanying the relativistic-like linear energy dispersion in graphene, with electrons traveling at a Fermi velocity only 100 times smaller than the speed of light, are its unique electronic and optical properties.[27,28] Intrinsic graphene has a universal optical conductivity of $e^2/4\hbar$, where $e$ is the electronic charge and $\hbar$ is the reduced Planck constant, hence, an absorption of $\alpha\pi \approx 2.3\%$ which depends only on the fine-structure constant $\alpha$.[29–32] Unlike metals, which have abundance of free charges, graphene is a semimetal. Free carriers can be induced through chemical doping or electrical gating with great ease due to its two-dimensional nature. Free carriers in graphene obtained through such means can reach around 0.001–0.01 per atom, or doping concentration of $1 \times 10^{12}$ to

* Address correspondence to tonyaslow@gmail.com, avouris@us.ibm.com.

Received for review December 27, 2013 and accepted January 28, 2014.

**Published online January 31, 2014**
10.1021/nn406627u

$1 \times 10^{13}$ cm$^{-2}$, which is significantly smaller than that of 1 per atom for noble metals. Solid electrolyte gating can allow for higher concentration of free carriers of 0.1 per atom, which translates to a chemical potential of $E_F \approx 1$ eV.[33] The two-dimensional and semimetallic nature of graphene, therefore, allows for electrical tunability not possible with conventional metals.

Figure 1a,b illustrates a characteristic absorption spectrum of graphene at finite doping and the different optical transition processes involved. The spectral weight below $2E_F$ is mainly imparted to a Drude peak response at terahertz frequencies, due to intraband free carriers absorption. At near-infrared to visible frequencies, absorption is due to direct interband transitions. In doped graphene at the mid-infrared regime, Pauli-blocking occurs and the optical conductivity is minimal. The residual absorption observed in experiments at low temperature[32] is generally attributed to disorder.[36] Graphene, besides being a unique material with unprecedented tunable optical properties, is also an excellent conductor of electricity. Highest attained carrier mobility has reached 1 000 000 cm$^2$/(V s) in suspended samples[37] and 100 000 cm$^2$/(V s) for ultraflat graphene on boron nitride.[38,39] These attributes, in addition to its stability and compatibility with standard silicon processing technologies, has led to the rapid development of promising graphene-based active devices on a silicon photonic platform, such as photodetectors in optical communication data-links[34,40] and electro-optical modulator in silicon waveguides,[35] among many others. Some of these active graphene devices are illustrated in Figure 1c,d. In similar fashion, the utilization of graphene plasmons, a collective form of electron excitation, allows for tunable plasmonic devices.

**VOCABULARY: Polaritons** - quasi-particles resulting from the coupling of electromagnetic waves and an electric dipole-carrying excitation such as phonon and plasmon. In graphene, these excitations reside in the terahertz to mid-infrared regime; **Terahertz radiations** - electromagnetic waves at wavelengths from 0.1 to 1 mm, while mid-infrared radiations from 3 to 8 $\mu$m. The following conversion can come in handy: 1 eV = 8000 cm$^{-1}$ = 1.25 $\mu$m = 240 THz;

**Terahertz to Mid-Infrared Plasmon–Polaritons.** Conventional plasmonics emerged from the early study of SPP confined to metallic surfaces,[41] where free electrons oscillate collectively in resonance with the electromagnetic field. They are confined transverse magnetic (TM)

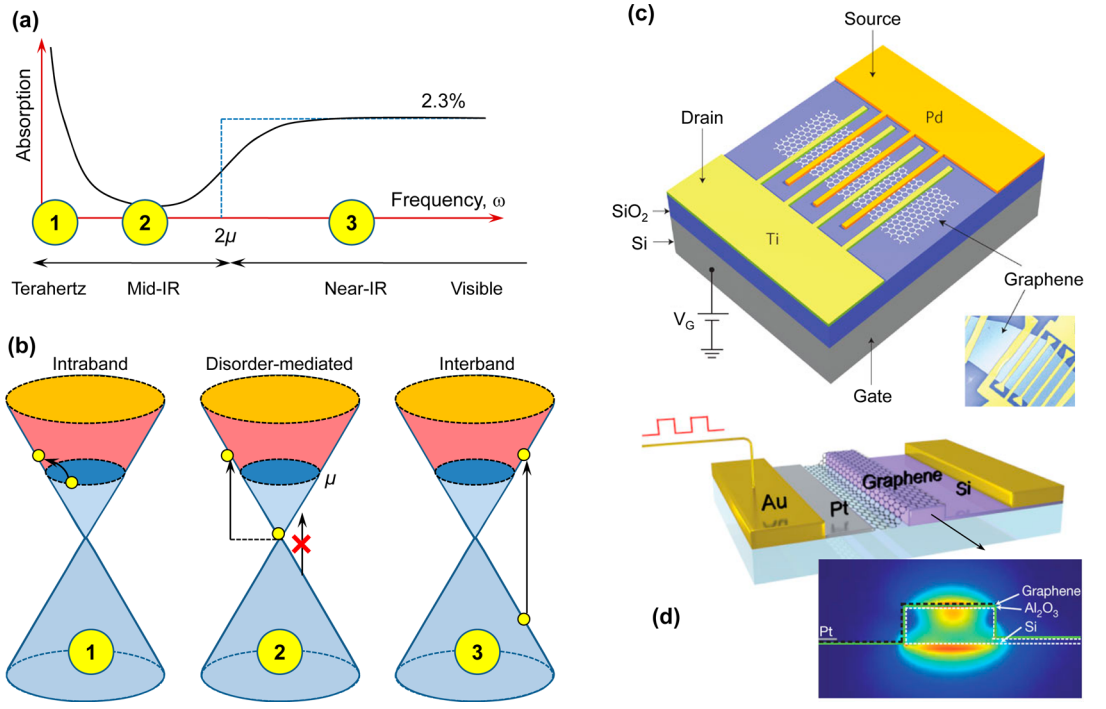


**Figure 1. (a) Illustration of a typical absorption spectrum of doped graphene.[29−32] It has characteristic features such as a Drude peak at terahertz frequencies, minimal absorption in the mid-infrared frequencies due to Pauli blocking and a transition to the universal 2.3% absorption beyond the far-infrared. (b) Illustration of the various optical transition processes. At small $\omega$ less than the thermal energy, transitions occur *via* intraband processes. At finite $\omega < 2\ \mu$, disorder plays an important role in imparting the momentum for the optical transition. A transition occurs around $\omega \approx 2\ \mu$, where direct interband processes lead to a universal 2.3% absorption. (c) Schematic of a metal–graphene–metal photodetector with asymmetric metal contacts, which was operated at 10 Gbits/s data rate with 1.55 $\mu$m light excitation as described in ref 34. (d) Schematic of a graphene-based waveguide-integrated optical modulator reported in ref 35. Inset shows a finite element simulation of the waveguide's optical mode, designed so as to maximize the field at the interface between the waveguide and the graphene for maximal absorption efficiency.**

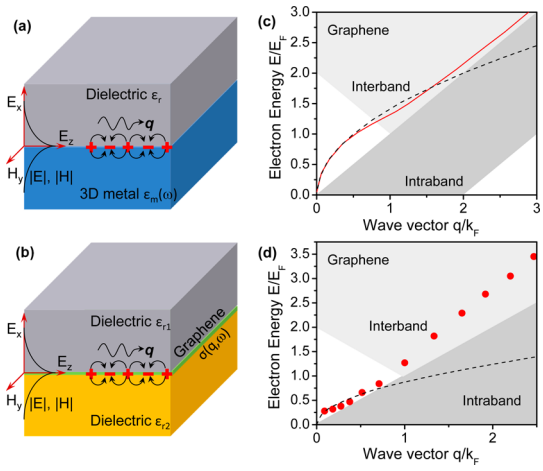


**Figure 2. (a) Illustration of a TM surface plasmon polariton (SPP) at a metal−dielectric interface. (b) Illustration of a TM plasmon mode in 2D graphene. (c) Plasmon dispersion in 2D graphene (solid line) calculated within the Random Phase Approximation (RPA) taken from ref 46. The dashed line indicates the long wavelength plasmon dispersion $\omega_{pl} \propto q$. Landau damping regions due to intraband and interband single particle electron−hole excitations are indicated. (d) Plasmon dispersion of 2D graphene on SiC(0001) (symbols) measured using EELS with data taken from ref 47. Dashed line is the long wavelength plasmon dispersion for reference.**

electromagnetic wave, where the electric field vector is parallel to the plasmon propagation direction *i.e.*, its wave vector **q**. This is illustrated in Figure 2a. The dispersion relation of this SPP mode is well-known, and can be obtained by solving Maxwell's equation under appropriate boundary conditions:[41,42]

$$q_{sp} = \frac{\omega}{c}\sqrt{\frac{\varepsilon_r \varepsilon_m(\omega)}{\varepsilon_r + \varepsilon_m(\omega)}} \quad (1)$$

where $\varepsilon_r = 1$ for air. A prerequisite for its existence is that $\varepsilon_r\varepsilon_m(\omega) < 0$; hence, metals are usually used. As an example, SPP at air−silver interface has the optimal electromagnetic wave confinement in the red part of the visible spectrum[20] *i.e.*, ≈18 000 $cm^{-1}$, with a wavevector $q_{sp}$ an order of magnitude larger than its free space momentum, *i.e.*, $q_0 = \omega/c$. Their weaker confinement and increased losses at lower frequencies make noble metal plasmons less appealing for applications at terahertz and mid-infrared frequencies.

The simple dielectric−graphene−dielectric system also accommodates a TM plasmon mode, as illustrated in Figure 2b. In the nonretarded regime where $q \gg q_0$, it has the following solution:[20,43,44]

$$q \approx \frac{i2\omega\varepsilon_r\varepsilon_0}{\sigma(q,\omega)} \quad (2)$$

where $\varepsilon_r$ is the average dielectric constant of its surrounding medium and $\sigma(q,\omega)$ is the nonlocal conductivity of graphene. In the long-wavelength (*i.e.*, $q \ll k_F$ where $k_F$ is the Fermi wave vector) and high doping (*i.e.*, $\hbar\omega \ll E_F$) limits, the conductivity is dominated by intraband electronic processes following the local Drude model,[45]

$$\sigma(\omega) = \frac{ie^2|E_F|}{\pi\hbar^2(\omega + i/\tau_e)} \quad (3)$$

Here, $\tau_e$ is the momentum relaxation time. Substituting eq 3 into eq 2, we obtain the plasmon dispersion relation in the long-wavelength limit,

$$q(\omega) = \frac{2\pi\hbar^2\varepsilon_0\varepsilon_r}{e^2E_F}\omega^2(1 + i/\tau\omega) = \frac{\varepsilon_r}{2\alpha}\frac{\omega}{\omega_F}k_0(1 + i/\tau\omega) \quad (4)$$

where $\alpha \equiv e^2/4\pi\hbar\varepsilon_0 c = 1/137$ is the fine strucure constant and $\omega_F = E_F/\hbar$. In the mid-infrared frequency, we have $\omega/\omega_F$ of order 1 under typical doping condition, implying a strong inherent plasmonic wave localization effect of order $1/\alpha$. Hence, the plasmon wavevector (momentum) $q$ in graphene can be two orders larger than $q_0$, which translates to a confinement volume $10^6$ times smaller than the diffraction limit. Such extreme light confinement effect makes graphene an attractive platform for nanophotonics in these spectral ranges *i.e.*, terahertz to mid-infrared. For clarity, the plasmon disperson $\omega_{pl}(q)$ from eq 4 can be obtained by setting $\tau_e = 0$,

$$\omega_{pl} = \sqrt{\frac{e^2E_Fq}{2\pi\hbar^2\varepsilon_0\varepsilon_r}} \quad (5)$$

The $\omega_{pl} \propto \sqrt{q}$ plasmon dispersion relation is expected for all 2D systems.[44] For example, when we use an electron concentration of $1 \times 10^{13}$ $cm^{-2}$, the plasmon frequency will reside in the mid-infrared regime of the electromagnetic spectrum.

**Coherent Plasmons Phase Space.** A plasmon, the quantum of plasma oscillation, can either be self-sustaining or severely damped. For technology, we are obviously interested in the former. Landau damping is a fundamental and intrinsic damping mechanism due to the loss of collective motion to the excitation of electron−hole pairs. This occurs when the phase space of plasmon and that of intraband and interband single particle electron−hole excitations overlaps as depicted in Figure 2c. It is also clear that the threshold for interband Landau damping can be tuned with $E_F$.

Electron energy loss spectroscopy (EELS) is a commonly used technique for the study of electronic and plasmonic properties of materials, including graphene films. The sample is exposed to a beam of electrons with well-defined kinetic energies, where the energy loss of the reflected or transmitted beam is then measured. A dominant source of energy loss is *via* the Coulomb interactions with the conduction electrons, including plasmons.[48,49] This energy loss can be computed within a rigorous and microscopic theoretical framework, the Random phase Approximation (RPA),[50−52] and is defined as the imaginary part of

the inverse dielectric function, *i.e.*, $L(q,\omega) \equiv \mathcal{J}[1/\varepsilon_{RPA}]$. $L(q,\omega)$ is known as the electron loss function. The dielectric function, in the absence of interactions, can be computed from,

$$\varepsilon_{RPA}(q,\omega) = \varepsilon_r - v_c \Pi^0_{\rho,\rho}(q,\omega) \quad (6)$$

where $v_c = e^2/2q\varepsilon_0$ is the 2D Coulomb interaction. $\Pi^0_{\rho,\rho}(q, \omega)$ is the 2D polarizability function which includes all single particle transitions between the various electronic bands. The mathematical details, including analytical form for $\Pi^0_{\rho,\rho}(q, \omega)$ derived at $T = 0$, are described in refs 46 and 53. However, in the regime in which we are interested, *i.e.*, $\omega > v_F q$ and $E_F \gg \hbar\omega$, $\Pi^0_{\rho,\rho}(q, \omega)$ can be approximated by,

$$\Pi^0_{\rho,\rho}(q,\omega) \approx \frac{E_F q^2}{\pi\hbar^2(\omega + i/\tau_e)^2} = \frac{\varepsilon_r}{v_c}\frac{\omega_{pl}^2}{\omega^2} \quad (7)$$

Collective plasmonic modes can then be obtained from the zeros of the full dielectric function *i.e.*, $\varepsilon_{RPA}(q,\omega) = 0$. From eqs 6 and 7, one arrived at the expected plasmon dispersion in the long-wavelength limit, $\omega = \omega_{pl}$.

Figure 2c shows the calculated plasmon dispersion from RPA theory using the exact form of $\Pi^0_{\rho,\rho}(q, \omega)$. At the long-wavelength limit, its dispersion follows the $\omega_{pl} \propto \sqrt{q}$ behavior expected for 2D plasmons.[44] However, departure from this $\sqrt{q}$ behavior becomes apparent at larger $q$, where it begins to acquire a more linear dispersion. EELS experiments were performed on single and multilayer doped graphene on a SiC(0001) crystalline wafer surface and also graphene grown on Cu foil by chemical vapor deposition (CVD),[47,54] where Figure 2d shows the measured graphene plasmon dispersion. EELS is not able to resolve plasmon dispersion at small $q$. At finite $q$, we see that it disperses rather linearly instead of the $\sqrt{q}$-dependence, due to nonlocal effects described within the RPA. At sufficiently large plasmon momentum, *i.e.*, $q > k_F$, the graphene plasmon enters the interband Landau damping regime, and becomes severely damped. By contrast, Landau damping for plasmons in conventional 2DEG occurs in the intraband regime instead, due to the presence of an energy gap. Note also the difference in the density dependence of $\omega_{pl}$ between graphene and 2DEG. As is apparent from eq 5, $\omega_{pl} \propto n^{1/4}$ in graphene while it varies as $\omega_{pl} \propto n^{1/2}$ in conventional 2DEG. One can show this by recasting into the conventional effective mass Drude model through the simple relations, $n = k_F^2/\pi$ and $m = E_F/v_F^2$.

So far, we discussed only the coherent plasmons due to intraband processes involving the $\pi$ band of graphene. However, graphene also accommodates energetically higher plasmonic modes, such as the $\pi$ and $\pi + \sigma$ plasmons at ≈5 and ≈15 eV, respectively.[55] These plasmonic modes arise from the $\pi$ band and interband processes with the high energy $\sigma$ band. However, these plasmonic modes reside within the Landau-damped regions, with measured full-width at half-maximum (fwhm) of the plasmon loss peak of order 1 to 10 eV.[47,54,55] As a result, they are not of interest to the plasmonic applications we are considering and will not be discussed further in this article.

**Confined Plasmon−Polaritons in Nanostructures.** The size of a material can influence how it interacts with light especially when it is much smaller than the free space wavelength. This fact was appreciated long ago by Mie,[57,58] when he explained the origin of the observed red color in spherical gold nanoparticles solution by simply solving Maxwell equation with the same bulk material dielectric properties, but with modified boundary conditions due to reduced size. Discontinuities in the electric permittivity can set up standing localized plasmon waves confined to the metal surfaces, when the light frequency is tuned to its plasmon resonance. In similar fashion, 2D localized plasmons can also be excited in lithographically designed thin film metal slabs, disks and their periodic arrays.[59−62]

Recently, localized plasmonic modes has been experimentally observed in graphene micro- to nanoribbons and nanodisks arrays,[21,22,63] through prominent absorption peaks in transmission spectroscopy measurements. In particular, polarization sensitive ribbon arrays provide a pedagogical framework for the study of basic properties of graphene plasmons,[22,63] as will be made apparent below. Electromagnetic simulations have shown that the plasmonic response between an individual ribbon and its arrays are indistinguishable, when the lattice constant of the array is more than twice the ribbons width,[64] implying that ribbon-to-ribbon coupling can be neglected in this limit. Plasmonic resonances within an individual ribbon occur when $q \approx (2n + 1)\pi/W$, where $W$ is the ribbon's width and $n = 0, 1, 2, \ldots$. This is the condition that the plasmon half-wavelengths will be able to fit within the ribbon width. Only plasmonic modes with odd multiples of half-wavelengths[65] couple with light as this produces an effective charge dipole that creates the necessary restoring force for collective charge oscillations.

Figure 3a,b illustrates the experimental measurement scheme used to study a graphene nanoribbon array on a diamond-like carbon (DLC) substrate as described in ref 22. The electromagnetic response of the array is characterized by its extinction spectrum, $Z(\omega) = 1 - T_{per}/T_{par}$, where $T_{per}$ and $T_{par}$ are the transmission of light through the ribbon array with electric field perpendicular and parallel to the ribbons. By excitating the localized plasmons, the extinction spectrum $Z(\omega)$ revealed prominent the resonant peaks shown in Figure 3c at room temperature. By contrast, analogous plasmonic absorption was observed in conventional two-dimensional electron gas systems only at 4.2 K.[66] The graphene plasmon dispersion $\omega_{pl}(q)$ can be mapped out by performing the measurement for

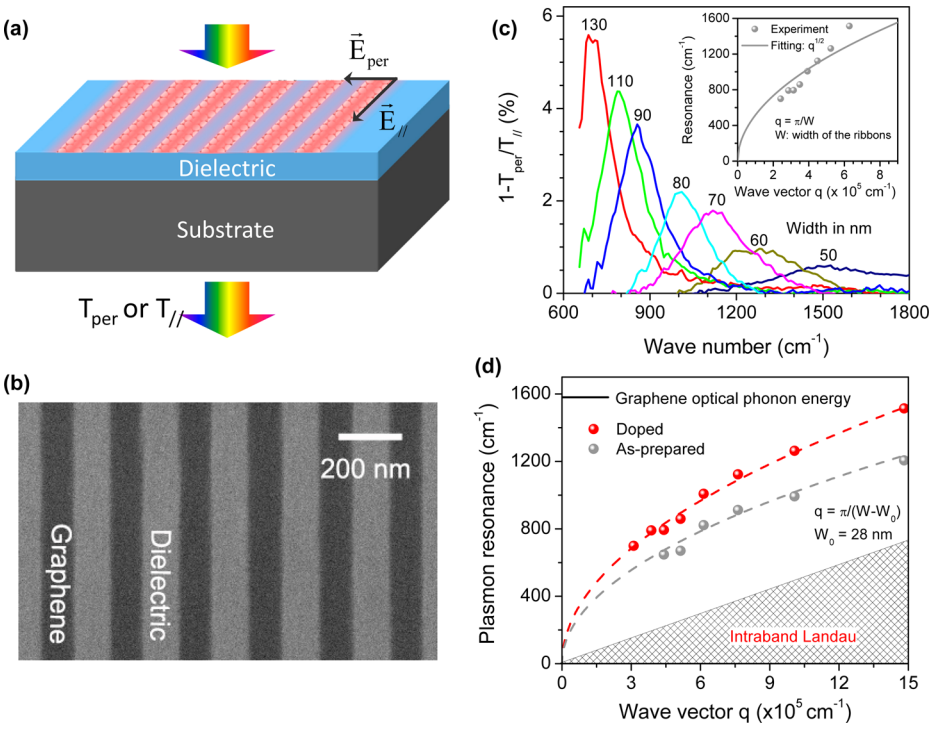


**Figure 3. (a) Mid-infrared transmission measurement setup for graphene nanoribbons, which also involves an infrared microscope coupled to a Fourier-transform infrared spectrometer (FTIR). (b) SEM image of an array of graphene nanoribbons with width of 100 nm. (c) Extinction spectra $Z(\omega) = 1 - T_{per}/T_{par}$, where $T_{per}$ and $T_{par}$ are the transmission of light through the ribbon array with electric field perpendicular and parallel to the ribbons. Inset: plasmon resonance frequency as a function of wave vector $q = \pi/W$, where $W$ is the width of the nanoribbon. The gray curve is a fit according to $\omega_{pl} \propto \sqrt{q}$. (d) The same plasmon resonance data (red dots) as in (c), now plotted as a function of wave-vector defined as $q = \pi/W_e$, where $W_e = W - W_0$ is an effective electrical width with $W_0 = 28$ nm. Plasmon resonance data for a lower Fermi level case are also plotted (gray dots). Dashed curves are again fitting to $\omega_{pl} \propto \sqrt{q}$. Figures are reprinted with permission from ref 22. Copyright 2013 Nature Publishing.**

ribbon arrays of different widths. When correction for an apparent difference between the electrical and physical width of the ribbons was done, a good agreement between the observed localized plasmon dispersion with the classical result of eq 4 was found as shown in Figure 3d. Unlike plasmonic resonances in metallic nanoparticles, graphene plasmons reside in the terahertz to mid-infrared regime. In addition, the two-dimensional and semimetallic nature of graphene allows for electrical tunability of these plasmonic resonances.[22,56,63,67]

**Seeing and Launching Propagating Plasmons.** Previously, we discussed how far-field scattered light produced by interaction with plasmons can allow one to derive information about the plasmonic behavior, such as its dispersion. Development of scanning near-field optical microscopy (SNOM)[68] has provided an opportunity for direct imaging of the SPP fields in conventional metal plasmonics with nanometer range resolution, where SPP scattering, interference effects and localization have been visualized.[69] Recently, a similar scattering-type SNOM has allowed for nanoimaging of infrared graphene plasmons[56,67] as illustrated in Figure 4a. Here, the sharp tip of an atomic force microscope, with radius of curvature $a \approx 25$ nm, is illuminated with a focused infrared beam, imparting the required momentum of order $1/a$ for the excitation of graphene plasmons. With the use of a free space incident light of wavelength 11.2 $\mu$m (or frequency $\omega = 892$ cm$^{-2}$), graphene plasmon in the form of a standing wave is observed. The graphene plasmon was found to have a wavelength of 200 nm, consistent with the estimate from eq 4 (here, graphene is supported on a $SiO_2$ substrate with a doping of $8 \times 10^{12}$ cm$^{-1}$), and 2 orders of magnitude smaller than the free space wavelength. Images of interference patterns generated by the plasmon wave close to the graphene edges, atomic defects, and at boundary of monolayer-bilayer graphene are displayed in Figure 4b–e.

The ability for controlled launching of propagating plasmons is a key element to nanophotonics applications. Conventional plasmonics approaches include the use of a prism, either in the Otto or Kretschmann configurations,[70,71] where the evanescent wave associated with total internal reflection excites propagating surface plasmons along the metal–dielectric interface. Excitation can also be performed using a diffraction grating, which shifts the wave-vector of incident electromagnetic wave to match that of the surface plasmon.[1] These techniques can also be applied to graphene,[72] among other proposed methods such as diffractive grating etched into the underlying

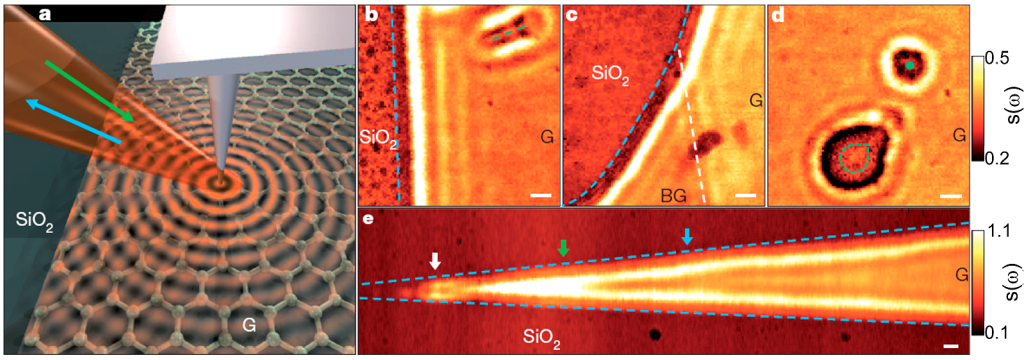


**Figure 4. (a) Diagram of an infrared nanoimaging experiment at the surface of graphene on $SiO_2$. Green and blue arrows display the directions of incident and backscattered light, respectively. Concentric red circles illustrate plasmon waves launched by the illuminated tip. (b–e) Images of infrared amplitude $s$ ($\omega$ = 892 cm$^{-1}$) defined in the text taken at zero gate voltage. These images show a characteristic interference pattern close to graphene edges (blue dashed lines) and defects (green dashed lines and green dot), and at the boundary between single and bilayer graphene (white dashed line). Locations of boundaries and defects were determined from AFM topography taken simultaneously with the near-field data. Scale bars, 100 nm. All data were acquired at ambient conditions. Figures are reprinted with permission from ref 56. Copyright 2012 Nature Publishing.**

substrate,[73,74] modulated conductivity in graphene[72] and *via* surface acoustic waves with a piezoelectric material.[75] Up to date, experimental demonstration of propagating graphene plasmons *via* these approaches has not yet been demonstrated.

**Coupling Plasmons with Phonons.** Atomic vibrations in polar crystals can also couple resonantly with electromagnetic fields. Hybridization between plasmons and the polar optical phonon modes has long been studied in the context of doped bulk semiconductors.[76] At the surfaces of these polar semiconductors, there are Fuchs-Kliewer surface optical (SO) phonons[77] which have been studied extensively in conventional two-dimensional electron gas system.[78] For isotropic polar dielectric material, the frequency of SO phonon is related to its bulk transverse and longitudinal optical (*i.e.*, TO and LO) phonons through $\omega_{SO} = [(\varepsilon_0 + 1)/(\varepsilon_\infty + 1)]^{1/2}\omega_{TO}$,[77] where $\varepsilon_0$ ($\varepsilon_\infty$) is the static (high frequency) dielectric constant and $\omega_{LO}/\omega_{TO} = (\varepsilon_0 + \varepsilon_\infty)^{1/2}$, *i.e.*, the Lyddane-Sachs-Teller relation. Recently, the potential benefits of coupling with these long-lived phonons for plasmonics applications have been recognized.[79−81] In addition, the surface polar phonon itself can be excited by light, forming phonon−polariton as demonstrated using infrared nanoscopy on SiC surfaces.[79]

When graphene is placed on a polar substrate, the electronic degrees of freedom in graphene, including its collective plasmon mode, can couple with these SO phonons as seen in recent experiments[22,47,82,83] *via* long-range Fröhlich coupling, leading to a modified plasmonic dispersion.[84] The dispersion of these coupled plasmon−phonon modes was recently measured.[22] In the experiment,[22] the extinction spectra for graphene ribbon arrays on a $SiO_2$ substrate with $W$ ranging from 60 to 240 nm were measured. There are three resonance peaks within the measured frequency range of 650−6000 cm$^{-1}$, due to the two relevant SO phonon modes of $SiO_2$ at 806 and 1168 cm$^{-1}$. The interaction of plasmon with these phonon modes can be described within a generalized RPA theory as described below. Figure 5a plots the measured resonances overlaid on the calculated RPA loss function with excellent agreement, where the strength of the plasmon-phonon coupling dictates the amount of anticrossing between the plasmon and phonon modes.

Dielectric function including electron coupling with these SO phonons can be written as (see also the Supplemental Information of ref 22):

$$\varepsilon_{RPA}(q,\omega) = \varepsilon_r - v_c\Pi^0_{\rho,\rho}(q,\omega) - \ldots \sum_{SO}\frac{\varepsilon_r\tilde{\omega}^2_{SO}}{(\omega+i/\tau_{SO})^2 - \omega^2_{SO} + \tilde{\omega}^2_{SO}} \quad (8)$$

where $\tau_{SO}$ is the lifetime of the SO phonon mode,

$$\tilde{\omega}_{SO} \equiv \sqrt{\frac{4\pi}{\hbar}\omega_{SO}\mathscr{F}^2} \quad (9)$$

$$\mathscr{F}^2 \equiv \frac{\hbar\omega_{SO}}{2\pi}\left(\frac{1}{\varepsilon_\infty + 1} - \frac{1}{\varepsilon_0 + 1}\right) \quad (10)$$

$\mathscr{F}^2$ describes the Fröhlich coupling strength, $\varepsilon_0$ ($\varepsilon_\infty$) are the low (high) frequency dielectric constant of the dielectric, which for $SiO_2$ is 3.9 (2.5). The frequencies of these coupled plasmon−phonon modes can be obtained by solving for $\varepsilon_{RPA} = 0$ numerically. In the simple case of only one SO mode, and setting $\tau_e = \tau_{SO} = 0$, the coupled plasmon−phonon modes reduces to a simple biquadratic equation given by,[22]

$$\omega^2_\pm = \frac{\omega^2_{pl} + \omega^2_{SO}}{2} \pm \frac{\sqrt{(\omega^2_{pl}+\omega^2_{SO})^2 - 4\omega^2_{pl}(\omega^2_{SO} - \tilde{\omega}^2_{SO})}}{2} \quad (11)$$

In the limit of zero coupling, *i.e.*, $\tilde{\omega}_{SO} \to 0$, we recover the expected limits $\omega_+ \to \omega_{SO}$ and $\omega_- \to \omega_{pl}$. The frequencies of these various SO phonon modes are the following: $\omega_{SO1} = 806$ cm$^{-1}$ and $\omega_{SO2} = 1168$ cm$^{-1}$.

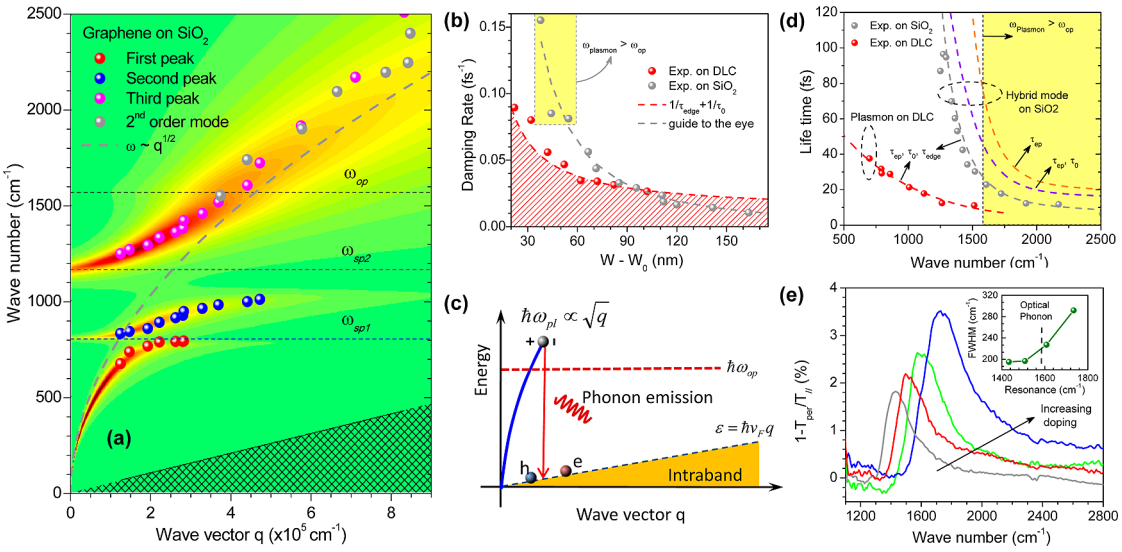


**Figure 5. (a) Plasmon frequency as a function of wave vector $q = \pi/W_e$ ($W_e$ is an effective electrical width) of hybrid plasmon−phonon coupled modes measured using the FTIR transmission spectroscopy technique. It is overlaid with the calculated loss function, plotted as a two-dimensional pseudocolor background. The dashed line represents the plasmon frequency without considering plasmon−phonon hybridization. Two surface polar phonons and the intrinsic optical phonon frequencies are indicated. (b) Damping rates of plasmons in graphene ribbons with similar doping on DLC (red) and $SiO_2$ (gray) as a function of $W_e$. For ribbons on $SiO_2$, peak 3 in (a) is analyzed. The red dashed curve gives the calculated damping rates including edge and the DC scattering time $\tau_0$. (c) Illustration of the plasmon damping process through the emission of an optical phonon, which brings it into the intraband Landau damping regime creating electron−hole pairs. (d) Plasmon lifetimes of ribbons on DLC (red dots) and $SiO_2$ (gray dots) as a function of plasmon resonance frequency. Dashed curves are calculated results including various scattering processes as described in the text. (e) Extinction spectra of a ribbon with width $W = 100$ nm on $SiO_2$ at 4 different doping levels. Inset shows the extracted fwhm as a function of the corresponding plasmon resonance frequency. Figures are reprinted with permission from ref 22. Copyright 2013 Nature Publishing.**

Typical quasi-particle lifetimes are $\tau_e = 0.1$ ps and $\tau_{SO} = 1$ ps. The coupling parameters obtained by fitting to experimental coupled plasmon−phonon resonances are $\mathcal{F}^2_{SO1} = 0.2$ meV and $\mathcal{F}^2_{SO2} = 2$ meV. Another SO phonon mode at $\omega_{SO} = 460$ cm$^{-1}$ (with $\mathcal{F}^2_{SO} = 0.2$ meV[85]) resides outside the experimental frequency range. Hence, the choice of substrate can be used to engineer the plasmon dispersion in graphene.

**Plasmon Damping Pathways and Lifetimes.** When the plasmon enters the phase space for single particle transitions (*i.e.*, intraband or interband), the plasmon dissociates into electron−hole pairs, losing its coherence and spectral weight. Plasmons can also decay into photons *via* radiative processes[86] which become insignificant in the electrostatic limit, *i.e.*, when the size of plasmonic structure is smaller than the wavelength of light. In addition, inelastic scattering with optical phonons and other carrier scattering processes can also contribute to plasmon damping. From the measured extinction spectra described above, the plasmon damping rate $\Gamma_{pl}$ can be extracted from the resonance line width, *i.e.*, full-width-half-maximum (fwhm), and is related to its lifetime *via* $\tau_{pl} = [2\Gamma_{pl}]^{-1}$.

Figure 5b,d shows the measured plasmon damping rate and lifetime is a function of both the ribbon's width and the plasmon frequency for both the graphene nanoribbons array on DLC and $SiO_2$ substrate. Here, the plasmon resides outside the Landau damping regions as shown in Figure 5a. A phenomenological model which reasonably accounts for the experimentally observed plasmon damping rate, $\Gamma_{pl}$, is given by,[22]

$$\Gamma_{pl}(\omega, W) = \Gamma_0(\omega) + \frac{2v_F}{W - W_0} \qquad (12)$$

$\Gamma_0$ characterizes the plasmon damping processes in bulk graphene, which includes scattering *via* optical phonons,[20,22] impurities,[87] defects[88] and electron−electron interactions.[89] The electron momentum relaxation time, $\tau_0$, obtained from dc Hall mobility measurements or the Drude peak in ac optical conductivity, provides reasonable estimates of the plasmon lifetime due to quasi-elastic processes. Electrical transport in large-scale grown CVD graphene and epitaxial graphene on SiC substrate are also affected by wrinkles[90] and atomic steps,[91] respectively, with measured electron mobility of order $\mu \approx 1000$ cm$^2$/(V s), which translates to $\tau_0 \approx 50$ fs. On the other hand, exfoliated graphene on boron nitride substrate can exhibit electron mobility of $\mu \approx 60\,000$ cm$^2$/(V s),[38] or $\tau_0 \approx 3$ ps.

However, highly inelastic processes due to intrinsic optical phonons, although not important at $\omega \rightarrow 0$,[92] can provide significant additional energy loss channel when the plasmon energy exceeds the optical phonon emission threshold, $\omega_{pl} > \omega_{op}$. The long-wavelength optical phonons in graphene are at an energy of $\omega_{op} = 0.2$ eV, or 1580 cm$^{-1}$. As shown in Figure 5d, the plasmon lifetime decays rapidly to 20 fs as its plasmon energy exceeds that of the optical phonon. This process

is schematically illustrated in Figure 5c, where through the emission of an optical phonon, the plasmon is brought into the intraband Landau damping regime with the creation of electron−hole pairs. Calculation of the plasmon lifetime due to this process, $\tau_{e-ph}(\omega)$, is described in detail in the Supplemental Information of refs 22 and 20. Evidence for the optical phonon mediated damping can be further strengthened by studying the carrier density dependence of the plasmon line width as shown in Figure 5e. As the plasmon frequency, which increases with doping, exceeds the graphene optical phonon energy, we observe a substantial increase in its resonance line width as shown in the inset of Figure 5d. This observation further reinforces our picture of the plasmon decay channel *via* optical phonon emission.

The latter contribution in eq 12 is a finite size effect resulting in plasmon lifetime of 50 fs for 100 nm width nanoribbons array. Ignoring other contributions, the plasmon damping due to this finite size effect goes as $1/q$, or inversely proportional to the confinement. This general trend has been observed in experiments.[93] Analogous finite-size effects also govern plasmon damping in metallic nanoparticles.[94] In this case, the damping is proportional to $1/r$, where $r$ is the radius of the nanoparticle. There are different physical models for this behavior, many of them summarized in ref 57, with the dominant mechanism depending on the particular experiment. The phenomenological model, eq 12, provides a satisfactory description of the experimentally observed graphene plasmon lifetime.

The role of phonons in the damping of plasmons is complex. Infrared phonons, such as the polar phonons in $SiO_2$, can couple remotely with the graphene plasmon. The resultant hybrid plasmon−phonon modes in turn inherit part of the long lifetime time of the phonon, typically of order of 1 ps. Analogous to a pair of classical coupled harmonic oscillators, the nature and quality of the coupled mode (that is, phonon- or plasmon-like) depends on its resonating frequency. For example, if it is resonating at a frequency close to one of the $SiO_2$ SO phonon, it would exhibit a narrower spectral width, inherited from the relatively long picosecond phonon lifetime. As shown in Figure 5d, the lifetime of the hybrid plasmon-phonon mode diverges at frequency close to one of the $SiO_2$ phonon at 1168 $cm^{-1}$.

The application of magnetic field can also strongly modify the plasmon lifetime. The cyclotron spectra of graphene in a nonquantizing magnetic field, $B$, given by $\omega_c = eB/m_c$, where $m_c = E_F/v_f^2$ is the cyclotron mass, which has a finite value dependent on the carrier density. In the absence of a magnetic field, the extinction spectra of an array of graphene microdisks measured with FTIR transmission spectroscopy technique reveal prominent resonance due to the localized 2D graphene plasmon.[95] The presence of a magnetic field would exert an additional cyclotron force, splitting the resonance into two peaks which move in opposite directions with increasing field,[95] with energies given by,

$$\omega_{\pm} = \sqrt{\omega_{pl}^2 + \omega_c^2/4} \pm \omega_c/2 \qquad (13)$$

where $\omega_{pl}$ is the localized plasmon in the absence of a magnetic field. Similar behavior was also observed at natural inhomogeneities (*e.g.*, step and wrinkles) on the graphene surface.[96]

The Faraday rotation spectra of these split magnetoplasmons show that each peak is excited by a different circular polarization direction. Most interestingly, the measured fwhm for $\omega_-$ becomes narrower while that of $\omega_+$ gets broader with increasing field.[95] With increasing magnetic field, the zero field plasmon splits into a bulk and an edge mode. The latter forms skipping orbits along the edges of the disks, effectively transforming the 2D plasmon into a 1D-like plasmon. Such edge current in a broken time reversal symmetric system has the characteristic of reduced backscattering, much akin to that of quantum Hall edge current, resulting in the reduced plasmon line width.[95] More recently, the edge plasmon dynamics in graphene disks were also measured using real time techniques.[97] The dramatic reduction in backscattering in the edge plasmon mode was verified and lifetimes as long as 50 ps (attenuation length of 70 ± 30 mm) were observed. This is about 3 orders of magnitude longer than the Drude relaxation time of the sample (0.05 ps for a sample mobility of 5000 $cm^2/(V\ s)$). Here, these measurements were performed under quantizing magnetic field for the $\nu = 2$ Landau level. The above results indicate that magnetic fields provide a powerful way of tuning not only the energy, but also the lifetime of plasmons in graphene.

**Enhanced Optoelectronics with Plasmons.** Graphene is a very unique optoelectronic material. Its large optical phonon energies ($E_{op}$ = 200 meV ≫ $kT$) and mismatch of Fermi and sound velocities ($v_F = 100v_s$) imply limited scattering phase space with its intrinsic phonons, which underlies the very weak electron−phonon coupling in graphene when compared to other material systems.[33,92] Hence, upon carrier excitation with light or other means, the electronic temperature in graphene can be driven far from equilibrium providing the potential for efficient optoelectronic devices.[85] The optoelectronic response in graphene can be driven by bolometric,[99,100] thermoelectric,[101,102] or photovoltaic[99,103] effects, depending on the device design and operating conditions. Due to the limited absorption of 2D graphene, its response is not particularly strong, and many strategies have been proposed to overcome this limitation. For example, microcavity-induced optical confinement leads to 20-fold enhancement in photocurrent,[104,105] silicon-waveguide-integrated graphene photodetectors

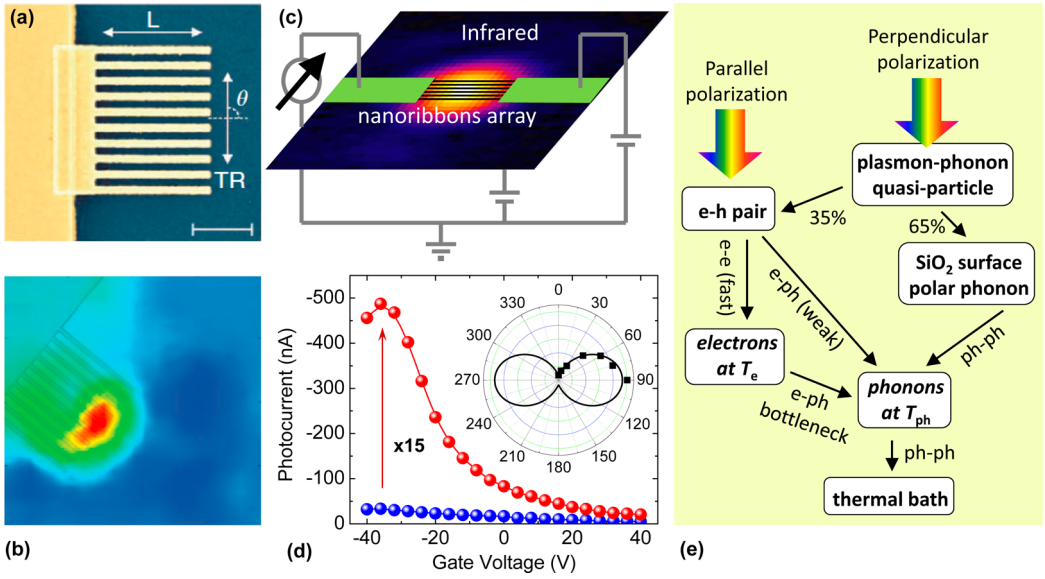


**Figure 6. (a) Scanning electron microscopy micrographs of the graphene devices with plasmonic nanostructures in false colors. Blue, graphene; purple, $SiO_2$ (300 nm); yellow, Ti/Au electrodes. Scale bar, 20 $\mu$m. (b) Photovoltage maps of the device with light polarization perpendicular to the ribbons excited at 514 nm. (c) Schematic of the photoconductivity setup with a graphene nanoribbon superlattice. Infrared laser light at 10.6 mm is chopped at 1.1 kHz and the photocurrent is analyzed by a lock-in amplifier referenced to the chopping frequency. (d) Gate-voltage-dependent photocurrent of a superlattice of 140 nm graphene nanoribbon array with incident infrared light polarization perpendicular (red spheres) and parallel (blue spheres) to the ribbons. Applied source-drain bias is 2 V. Inset shows the polarization dependence of the peak photocurrent under the same conditions. (e) Illustration of the mechanism of phonon and hot electron generation through decay of the hybrid plasmon−phonon quasi-particles. Perpendicular polarization excites primarily the plasmon−phonon mode, while parallel polarization excites individual electron−hole pairs. The plasmon−phonon quasi-particle decays mainly through SO phonons into other phonons, while electron−hole pairs decay primarily into hot electrons. Electrons thermalize among themselves at a temperature $T_e$ and phonons among themselves at a temperature $T_{ph}$. A bottleneck exists between electron and phonon baths, preventing full equilibration of electrons and phonons in graphene. Relevant scattering mechanisms (electron−electron, electron−phonon or phonon−phonon) are indicated. Figures are reprinted with permission from refs 98 and 23. Copyright 2011 and 2013, respectively, Nature Publishing.**

also improves responsivities,[106,107] and by integrating metallic plasmonic nanostructures with graphene photodetectors as depicted in Figure 6a,b, an order of magnitude enhancement in photoresponsivity has been achieved.[98,108] Engineering the physical dimension of metallic plasmonic nanostructures allows for spectral selective amplification of photoresponse. Research efforts have focused primarily on the near-infrared to visible regions mainly for applications in optical communications.

The terahertz and mid-infrared bands are important spectral ranges where more efficient and compact imaging and sensing devices are needed for critical security and local communications applications. Although state-of-the-art infrared detectors based on semiconductor quantum well photoconductors have response time and sensitivity approaching fundamental limits, they require cryogenic temperature operation at 4.2 K.[109] Utilizing graphene's intrinsic plasmons would enable tunable enhanced light absorption, especially in the mid and far-infrared range.[32] Gate-tunable plasmonic enhanced photodetection at room temperature in the mid-infrared regime with graphene nanoribbons array was recently demonstrated.[23] This is illustrated in Figure 6c,d. Here, a hybrid plasmon−phonon mode is excited at 943 $cm^{-1}$ with a $CO_2$ laser (with perpendicular polarization), which upon decay raises both the electron and phonon temperatures ($T_e$ and $T_{ph}$). The elevated temperature then produces a change in the electrical conductivity and, hence, a change in the photocurrent. A schematic of the photocurrent generation mechanism is shown in Figure 6e. Despite this being the first demonstration of optoelectronic response driven by intrinsic plasmons in graphene metamaterials, the observed photoresponse enhancement is already more than an order of magnitude under ambient conditions for a 140 nm nanoribbons array as shown in Figure 6d. In addition, the narrow line width of ≈100 meV further allows for gate-controlled switching of the plasmonic effect.

**Active Metamaterials.** Metamaterials are artificially structured materials with engineered electromagnetic properties not commonly found in nature, such as negative index-of-refraction,[6] electromagnetically induced transparency (EIT),[7] superlensing[8] and cloaking.[9] Since the electromagnetic response of metamaterials can be tailored to a particular region of the electromagnetic spectrum, especially the "terahertz gap" (0.1−10 THz) region where most of naturally occurring materials are unresponsive, metamaterials are playing an increasingly important role in creating necessary functional devices for the rapidly developing terahertz

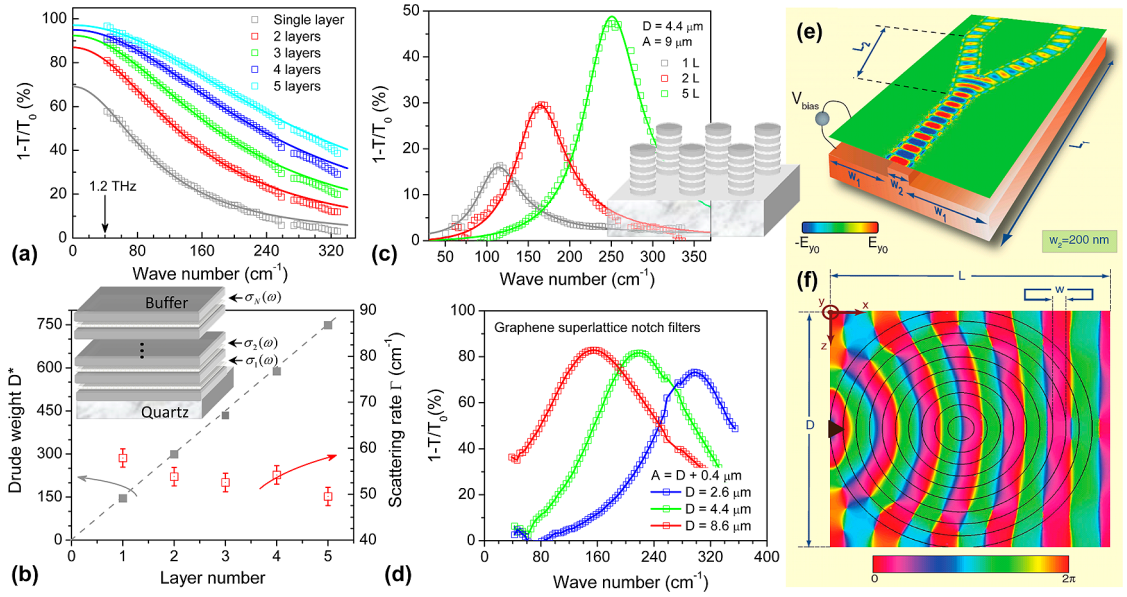


**Figure 7. (a) Terahertz electromagnetic wave shielding using transparent graphene/insulator stacks as illustrated in the inset of (b). Extinction spectra quantify the shielding effectiveness using stacked devices with one, two, three, four and five layers of graphene. Solid lines are fitted curves. (b) Fitted Drude weight and scattering width as a function of graphene layer number in the stacked devices. The Drude weight increases linearly with layer number, while the scattering width stays constant. (c) Plasmons in patterned graphene/insulator stacks. Extinction in transmission in stacked plasmonic devices with one, two and five graphene layers. The graphene plasmonic device is formed by patterning the stacked layers into microdisks in a triangular lattice as shown in the inset, where *d* is the diameter of the disk and *a* is the lattice constant of the array. (d) Extinction spectra of tunable terahertz filters using stacked devices with five graphene layers. The resonance frequency can be tuned by varying the diameter *d* of the disks. In these filters, the lattice constant *a* is always 400 nm larger than the disk diameter *d*. (e) Guiding of plasmon in 2D graphene utilizing spatially varying conductivity (or doping) through different capacitive coupling to the underlying back-gate. Simulation results of the electric field component $E_y$ (snapshot in time) for an infrared-guided wave at frequency of 30 THz with the ribbon-like section split into two paths. (f) Implementation of transformation optics in 2D graphene. Here a simulation shows a 2D version of the Luneburg lens of the phase of $E_y$ at frequency of 30 THz. Panels a–d are reprinted with permission from ref 21. Copyright 2012 Nature Publishing. Panels e and f are reprinted with permission from ref 110. Copyright 2011 The American Association for the Advancement of Science.**

technologies.[24] Terahertz functional devices including phase and amplitude modulators based on metallic metamaterials on Schottky diode structures[111,112] and narrow-band perfect absorbers[113] have been demonstrated, but with limited active electrical tunability at room temperature.

Graphene metamaterials offer a very wide design space for functional devices. Examples involve tunable graphene/insulator stacks, far-infrared notch filters with 8.2 dB rejection ratios and capable of shielding 97.5% of the incoming terahertz radiation, while at the same time remaining relatively transparent elsewhere,[21] as illustrated in Figure 7a,b. Better shielding can be achieved with increasing layer number *N*, since the Drude weight scales linearly with *N* as shown in Figure 7b. Transparent far-infrared filters can also be implemented with similar graphene/insulator stacks in the form of microdisk arrays as illustrated in Figure 7c, d. Here, electromagnetic resonances can be tuned through various means. For example, the plasmon resonance increases with $1/\sqrt{d}$ where *d* is the structural size, with the carrier density as $n^{1/4}$ and $n^{1/2}$ for single and stacked graphene layers, respectively,[114] with the number of stacked graphene layers as $N^{1/2}$, or *via* interdisk interaction through varying the lattice constant *a*. Figure 7c,d illustrates two particular examples of tuning, by varying *a* and *d*, respectively. In principle, varying the doping and microstructure dimensions would enable devices with electromagnetic response ranging from terahertz to mid-infrared, operating at room temperature. Simple graphene micro- and nanoribbons arrays have also allowed the realization of terahertz to mid-infrared linear polarizers with extinction ratio of ≈90%.[22,63] Integrating graphene with an array of meta-atoms and metallic wire gate electrodes, gate-controlled graphene-based metamaterials allow for modulation of both the amplitude and phase of transmitted terahertz wave by up to 47% and 32.2°, respectively.[115] Furthermore, the tunability of graphene provides a way to dynamically control the phase of a reflected electromagnetic field. Using an array of reflective cells, which individually produce a specific phase-shift upon reflection of the wave, would allow the construction of a desirable far-field beam, with applications as reflectarray antennas,[116–118] *e.g.*, for space applications. Various theoretical proposals, yet to be experimentally demonstrated, include complete optical absorption,[119] graphene mantle cloak,[120] transformation optics,[110] hyperbolic metamaterials and hyperlenses based on graphene–insulator stacks.[121,122]

Figure 7e,f shows two illustrative examples of transformation optics using graphene,[110] by designing and manipulating spatially inhomogeneous nonuniform conductivity patterns across the 2D graphene.

**Mid-Infrared Vibrational Spectroscopy.** Vibrational spectra provide fingerprints of molecular structures and as such they are used extensively in science and technology. The two techniques commonly used to obtain vibrational spectra are infrared absorption spectroscopy and Raman scattering.[125] Nanoscience and technology demands spectroscopy on smaller and smaller samples and even single molecules[16] and there is increasing need for better detectivity of vibrational spectra. Plasmonic effects have served as a powerful means to enhance optical fields and are utilized in various surface-enhanced optical phenomena such as Raman scattering and second harmonic generation.[126] In general, the effectiveness of a plasmonic system to enhance the optical field is often expressed by its quality factor $Q$, given by $Q = -\mathrm{Re}[\varepsilon_m]/\mathrm{Im}[\varepsilon_m]$, where $\varepsilon_m$ is the complex dielectric function of the metal particle. In the case of noble metal plasmonic systems, $Q$ is in the range of 10−100, and the local optical field intensity enhancement responsible for the increase in absorption/emission rates is proportional to $Q^2$, and $Q^4$ for Raman scattering.

In metal particles, the plasmon resonance occurs when $|\varepsilon_m + \varepsilon_s|$ is minimum, where $\varepsilon_s$ is the dielectric function of the surrounding medium.[57] For noble metals (Au and Ag), the plasmon resonances are typically in the visible part of the spectrum, while molecular vibrational mode frequencies are in the mid-infrared. These plasmonic resonances could be red-shifted up to the near-infrared by modifying the dielectric environment, *e.g.*, by coating with a high permittivity dielectric.[127] By switching from spherical to ellipsoidal particles, the fundamental plasmonic mode can be split into two branches, with the low-energy resonance occurring when the length of the rod is a multiple of the exciting wavelength.[128,129] Figure 8a shows a periodic array of gold plasmonic nanorods designed for the detection of vibrational modes of a protein monolayer.[123] It has a plasmonic resonance which resides close to two vibrational modes of the silk fibroin protein at 1537 and 1660 $cm^{-1}$, see also inset of Figure 8b. The measured reflectance spectra in Figure 8b show clear signatures of these vibrational modes for just a 2 nm thick protein film. In graphene nanoribbons and microribbons, localized plasmon resonances can occur in the near-infrared to far-infrared. In addition, the graphene plasmon resonance is tunable by changing the carrier density electrostatically or chemically. This invokes the interesting possibility of using patterned graphene or graphene on grating structures for mid-infrared vibrational spectroscopy of absorbed molecules. Figure 8c illustrates a schematic of such an application.[124] Below,

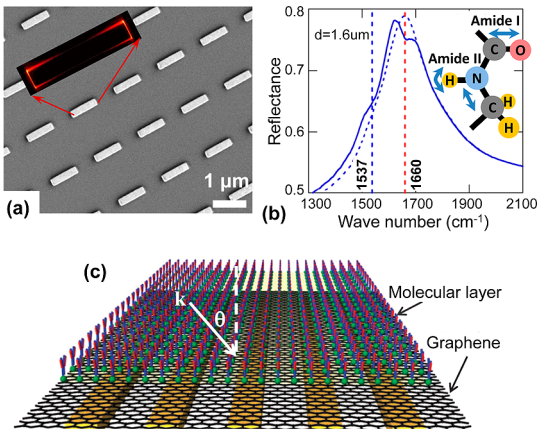


**Figure 8. (a) Scanning electron micrograph of a periodic array of gold nanorods designed such that their plasmonic resonance resides near the vibrational modes of a silk fibroin protein sample. Inset shows the simulated field intensity around the rod. (b) Reflectance spectra from a 1.6 $\mu$m periodic array before (dashed line) and after coating it with a 2 nm thick protein film (solid line). The amide-I and II vibrational modes of the protein backbone are illustrated in the inset. (c) Illustration of a graphene grating structure used for the excitation of plasmons and the detection of thin film molecular layers. Panels a and b are reprinted with permission from ref 123. Copyright 2009 The Proceedings of the National Academy of Science. Panel c is reprinted with permission from ref 124. Copyright 2013 American Physical Society.**

we consider a pedagogical example which illustrates the basic principles of how plasmons in graphene can be used to enhance the infrared activity of phonons.

Consider graphene's immediate cousin: its AB Bernal-stacked bilayer version.[130−132] In monolayer graphene, the in-plane optical phonon at the $\Gamma$ point does not have any infrared activity. However, in bilayer, the $\Gamma$ phonons of the two layers can couple to form an in-phase (symmetric) and an out-of-phase (antisymmetric) mode, where inversion symmetry is no longer invariant in the latter.[133] As a result, the antisymmetric mode becomes infrared active. It appears as a peak in absorption absorption at $\omega \approx 0.2$ eV, with a strong dependence of the peak intensity and of its Fano-type line shape on the applied gate voltage.[134,135] In the absence of any plasmonic enhancement, the measured extinction of this infrared-active phonon mode in bilayer is about 1%.[134−136] Plasmons in bilayer graphene nanostructures can enhance the phonon infrared activity, as shown in a most recent experiment,[136] achieving at least a 5-fold enhancement of the measured extinction.

The effect of electron−phonon interaction on the plasmonic response of graphene can be described within the RPA formalism, according to the charged-phonon model.[137,138] Renormalized by many-body interactions, this 'dressed' phonon gives rise to a Fano asymmetric spectral line shape. The Fano feature develops as a result of the interference between the discrete phonon mode and the 'leaky' plasmonic

mode; the electronic lifetime is significantly shorter than that of the phonon, broadening the former into a quasi-continuum. At zero detuning, a very narrow transparent window emerges within the broadly opaque plasmonic absorpion.[136,138] This enhancement of infrared phonon spectral weight with decreasing detuning underlies the basic physics of plasmon enhanced infrared spectroscpy.[139] Similarly, this basic principle can also be extended to that of mid-infrared vibrational spectroscopy of absorbed molecules as illustrated in Figure 8c. In this case, the infrared phonon (vibration) resides outside of graphene where the plasmon−phonon interaction is remote, but the physical principle is the same. Indeed, recent classical electromagnetic calculations[124] of the system in Figure 8c reveal similar type of Fano line shape and transparency features. Other calculations suggest giant levels of light concentration leading to huge infrared-absorption enhancement in certain graphene nanostructures.[140]

## CONCLUDING REMARKS

In summary, there are a number of unique properties of graphene plasmonics that distinguish it from conventional metal plasmonics and many new possible areas of applications. First, the two types of plasmonics materials are fundamentally different. Graphene is the ultimate thin 2D material, covalent, flexible and inert, which can be fabricated and patterned using standard techniques such as CVD growth, lithography and etching. The energy of graphene plasmons is tunable either by electrostatic (gate) or chemical doping. Unlike noble metal plasmons whose prime application range is in the visible part of the spectrum, graphene plasmonics operate at long wavelengths: middle, far-infrared, and terahertz ranges. This enables infrared photonic applications (*e.g.*, infrared photodetection, enhanced infrared absorption, optical communications) and helps to bridge the so-called THz gap. Moreover, graphene is compatible with silicon electronics and photonics and can be incorporated in these technologies. It can also be used in conjunction with conventional metamaterials and structures, such as nanoantennas, to confer to them the desired tunability, while the high sensitivity of the graphene surface plasmons to changes in the environment (changes in the dielectric function or charge transfer) suggest sensitive sensor capabilities.

To fully exploit the possibilies offered by graphene plasmonics, a number of advances are required. First, more fundamental science work is needed to fully understand the behavior of plasmons in both monolayer and multiple layer graphenes, in particular the damping processes. The detailed behavior of these plasmons is largely determined by the quality of the graphene itself. Large-scale grown high quality graphene is highly desirable in many of the applications we discussed. Advances in the high quality graphene growth and in the passivation chemistry of edges would reduce scattering and increase the Q-factors of the corresponding plasmonic devices. Development of controllable and stable chemical doping for graphene is highly desirable. While use of localized plasmons in patterned graphene provides a very convenient way of optically accessing these excitations, edge-scattering increases their damping rates. For this reason, alternative ways of exciting plasmons in extended graphene such as the use patterned substrates, *e.g.*, gratings, should be pursued.

At the same time, we should be reminded that graphene is only a particular example of 2D van der Waals layered materials. In the larger picture, we have other 2D materials such as boron nitride,[141] transition metal dichalcogenides,[141−143] metallic oxides[144] and many others. These materials include metals, semimetals, semiconductors, topological insulators, and common insulators, including hybrid heterostructures,[141−145] and come with interesting electrical and optical properties.[146−150] From this standpoint, the research on graphene plasmonics is a precursor to plasmonics with 2D materials, most of which are unexplored to-date. These diverse material properties allow for different and new application space beyond what conventional bulk metal plasmonics material can possibly offer.

*Conflict of Interest:* The authors declare no competing financial interest.

*Acknowledgment.* The authors are grateful for the fruitful collaboration and discussions with Hugen Yan, Marcus Freitag, Fengnian Xia, Francisco Guinea, Damon Farmer and Wenjuan Zhu.

## REFERENCES AND NOTES

1. Maier, S. A. *Plasmonics: Fundamentals and Applications*; Springer: New York, 2007.
2. Pines, D. *Elementary Excitations in Solids: Lectures on Phonons, Electrons, and Plasmons*; Westview Press: Boulder, CO, 1999; Vol. 5.
3. Gramotnev, D. K.; Bozhevolnyi, S. I. Plasmonics Beyond the Diffraction Limit. *Nat. Photonics* **2010**, *4*, 83–91.
4. Novotny, L.; van Hulst, N. Antennas for Light. *Nat. Photonics* **2011**, *5*, 83–90.
5. Schuller, J. A.; Barnard, E. S.; Cai, W.; Jun, Y. C.; White, J. S.; Brongersma, M. L. Plasmonics for Extreme Light Concentration and Manipulation. *Nat. Mater.* **2010**, *9*, 193–204.
6. Shalaev, V. M. Optical Negative-Index Metamaterials. *Nat. Photonics* **2007**, *1*, 41–48.
7. Luk'yanchuk, B.; Zheludev, N. I.; Maier, S. A.; Halas, N. J.; Nordlander, P.; Giessen, H.; Chong, C. T. The Fano Resonance in Plasmonic Nanostructures and Metamaterials. *Nat. Mater.* **2010**, *9*, 707–715.
8. Kawata, S.; Inouye, Y.; Verma, P. Plasmonics for Near-Field Nano-Imaging and Superlensing. *Nat. Photonics* **2009**, *3*, 388–394.
9. Cai, W.; Chettiar, U. K.; Kildishev, A. V.; Shalaev, V. M. Optical Cloaking with Metamaterials. *Nat. Photonics* **2007**, *1*, 224–227.
10. Kabashin, A. V.; Evans, P.; Pastkovsky, S.; Hendren, W.; Wurtz, G. A.; Atkinson, R.; Pollard, R.; Podolskiy, V. A.;

Zayats, A. V. Plasmonic Nanorod Metamaterials for Biosensing. *Nat. Mater.* **2009**, *8*, 867–871.
11. Xu, H.; Bjerneld, E. J.; Kll, M.; Brjesson, L. Spectroscopy of Single Hemoglobin Molecules by Surface Enhanced Raman Scattering. *Phys. Rev. Lett.* **1999**, *83*, 4357.
12. Atwater, H. A.; Polman, A. Plasmonics for Improved Photovoltaic Devices. *Nat. Mater.* **2010**, *9*, 205–213.
13. Chang, D. E.; Srensen, A. S.; Demler, E. A.; Lukin, M. D. A Single-Photon Transistor Using Nanoscale Surface Plasmons. *Nat. Phys.* **2007**, *3*, 807–812.
14. Gonzalez-Tudela, A.; Martin-Cano, D.; Moreno, E.; Martin-Moreno, L.; Tejedor, C.; Garcia-Vidal, F. J. Entanglement of Two Qubits Mediated by One-Dimensional Plasmonic Waveguides. *Phys. Rev. Lett.* **2011**, *106*, 020501.
15. Kneipp, K.; Wang, Y.; Kneipp, H.; Perelman, L. T.; Itzkan, I.; Dasari, R. R.; Feld, M. S. Single Molecule Detection Using Surface-Enhanced Raman Scattering (Sers). *Phys. Rev. Lett.* **1997**, *78*, 1667.
16. Nie, S.; Emory, S. R. Probing Single Molecules and Single Nanoparticles by Surface-Enhanced Raman Scattering. *Science* **1997**, *275*, 1102–1106.
17. West, P. R.; Ishii, S.; Naik, G. V.; Emani, N. K.; Shalaev, V. M.; Boltasseva, A. Searching for Better Plasmonic Materials. *Laser Photonics Rev.* **2010**, *4*, 795–808.
18. Grigorenko, A. N.; Polini, M.; Novoselov, K. S. Graphene Plasmonics. *Nat. Photonics* **2012**, *6*, 749–758.
19. Koppens, F. H.; Chang, D. E.; de Abajo, F. J. G. Graphene Plasmonics: A Platform for Strong LightMatter Interactions. *Nano Lett.* **2011**, *11*, 3370–3377.
20. Jablan, M.; Buljan, H.; Soljacic, M. Plasmonics in Graphene at Infrared Frequencies. *Phys. Rev. B: Condens. Matter* **2009**, *80*, 245435.
21. Yan, H.; Li, X.; Chandra, B.; Tulevski, G.; Wu, Y.; Freitag, M.; Zhu, W.; Avouris, P.; Xia, F. Tunable Infrared Plasmonic Devices Using Graphene/Insulator Stacks. *Nat. Nanotechnol.* **2012**, *7*, 330–334.
22. Yan, H.; Low, T.; Zhu, W.; Wu, Y.; Freitag, M.; Li, X.; Guinea, F.; Avouris, P.; Xia, F. Damping Pathways of Mid-Infrared Plasmons in Graphene Nanostructures. *Nat. Photonics* **2013**, *7*, 394–399.
23. Freitag, M.; Low, T.; Zhu, W.; Yan, H.; Xia, F.; Avouris, P. Photocurrent in Graphene Harnessed by Tunable Intrinsic Plasmons. *Nat. Commun.* **2013**, *4*, No. 1951.
24. Tonouchi, M. Cutting-Edge Terahertz Technology. *Nat. Photonics* **2007**, *1*, 97–105.
25. Ferguson, B.; Zhang, X.-C. Materials for Terahertz Science and Technology. *Nat. Mater.* **2002**, *1*, 26–33.
26. Soref, R. Mid-Infrared Photonics in Silicon and Germanium. *Nat. Photonics* **2010**, *4*, 495–497.
27. Geim, A. K.; Novoselov, K. S. The Rise of Graphene. *Nat. Mater.* **2007**, *6*, 183–191.
28. Neto, A. C.; Guinea, F.; Peres, N. M. R.; Novoselov, K. S.; Geim, A. K. The Electronic Properties of Graphene. *Rev. Mod. Phys.* **2009**, *81*, 109.
29. Kuzmenko, A. B.; Heumen, E. V.; Carbone, F.; Marel, D. V. D. Universal Optical Conductance of Graphite. *Phys. Rev. Lett.* **2008**, *100*, 117401.
30. Mak, K. F.; Sfeir, M. Y.; Wu, Y.; Lui, C. H.; Misewich, J. A.; Heinz, T. F. Measurement of the Optical Conductivity of Graphene. *Phys. Rev. Lett.* **2008**, *101*, 196405.
31. Nair, R. R.; Blake, P.; Grigorenko, A. N.; Novoselov, K. S.; Booth, T. J.; Stauber, T.; Peres, N. M. R.; Geim, A. K. Fine Structure Constant Defines Visual Transparency of Graphene. *Science* **2008**, *320*, 1308–1308.
32. Li, Z. Q.; Henriksen, E. A.; Jiang, Z.; Hao, Z.; Martin, M. C.; Kim, P.; Stormer, H. L.; Basov, D. N. Dirac Charge Dynamics in Graphene by Infrared Spectroscopy. *Nat. Phys.* **2008**, *4*, 532–535.
33. Efetov, D. K.; Kim, P. Controlling Electron-Phonon Interactions in Graphene at Ultrahigh Carrier Densities. *Phys. Rev. Lett.* **2010**, *105*, 256805.
34. Mueller, T.; Xia, F.; Avouris, P. Graphene Photodetectors for High-Speed Optical Communications. *Nat. Photonics* **2010**, *4*, 297–301.
35. Liu, M.; Yin, X.; Ulin-Avila, E.; Geng, B.; Zentgraf, T.; Ju, L.; Wang, F.; Zhang, X. A Graphene-Based Broadband Optical Modulator. *Nature* **2011**, *474*, 64–67.
36. Yuan, S.; Roldn, R.; Raedt, H. D.; Katsnelson, M. I. Optical Conductivity of Disordered Graphene Beyond the Dirac Cone Approximation. *Phys. Rev. B: Condens. Matter* **2011**, *84*, 195418.
37. Du, X.; Skachko, I.; Barker, A.; Andrei, E. Y. Approaching Ballistic Transport in Suspended Graphene. *Nat. Nanotechnol.* **2008**, *3*, 491–495.
38. Dean, C. R.; Young, A. F.; Meric, I.; Lee, C.; Wang, L.; Sorgenfrei, S.; Watanabe, K.; *et al.* Boron Nitride Substrates for High-Quality Graphene Electronics. *Nat. Nanotechnol.* **2010**, *5*, 722–726.
39. Mayorov, A. S.; Gorbachev, R. V.; Morozov, S. V.; Britnell, L.; Jalil, R.; Ponomarenko, L. A.; Blake, P.; *et al.* Micrometer-Scale Ballistic Transport in Encapsulated Graphene at Room Temperature. *Nano Lett.* **2011**, *11*, 2396–2399.
40. Xia, F.; Mueller, T.; ming Lin, Y.; Valdes-Garcia, A.; Avouris, P. Ultrafast Graphene Photodetector. *Nat. Nanotechnol.* **2009**, *4*, 839–843.
41. Maier, S. A.; Atwater, H. A. Plasmonics: Localization and Guiding of Electromagnetic Energy in Metal/Dielectric Structures. *J. Appl. Phys.* **2005**, *98*, 011101.
42. Barnes, W. L.; Dereux, A.; Ebbesen, T. W. Surface Plasmon Subwavelength Optics. *Nature* **2003**, *424*, 824–830.
43. Mikhailov, S. A.; Ziegler, K. New Electromagnetic Mode in Graphene. *Phys. Rev. Lett.* **2007**, *99*, 016803.
44. Stern, F. Polarizability of a Two-Dimensional Electron Gas. *Phys. Rev. Lett.* **1967**, *18*, 546–548.
45. Peres, N. M. R. Colloquium: The Transport Properties of Graphene: An Introduction. *Rev. Mod. Phys.* **2010**, *82*, 2673.
46. Hwang, E. H.; Sarma, S. D. Dielectric Function, Screening, and Plasmons in Two-Dimensional Graphene. *Phys. Rev. B: Condens. Matter* **2007**, *75*, 205418.
47. Liu, Y.; Willis, R. F.; Emtsev, K. V.; Seyller, T. Plasmon Dispersion and Damping in Electrically Isolated Two-Dimensional Charge Sheets. *Phys. Rev. B: Condens. Matter* **2008**, *78*, 201403.
48. Pines, D.; Bohm, D. A Collective Description of Electron Interactions: II. Collective *vs* Individual Particle Aspects of the Interactions. *Phys. Rev.* **1952**, *85*, 338.
49. Ritchie, R. H. Plasma Losses by Fast Electrons in Thin Films. *Phys. Rev.* **1957**, *106*, 874.
50. Bruus, H.; Flensberg, K. *Many-Body Quantum Theory in Condensed Matter Physics: An Introduction*; Oxford University Press: Oxford, 2004.
51. Giuliani, G. F. *Quantum Theory of the Electron Liquid*; Cambridge University Press: Cambridge, 2005.
52. Mahan, G. D. *Many Particle Physics*; Springer: New York, 2000.
53. Wunsch, B.; Stauber, T.; Sols, F.; Guinea, F. Dynamical Polarization of Graphene at Finite Doping. *New J. Phys.* **2006**, *8*, 318.
54. Shin, S. Y.; Kim, N. D.; Kim, J. G.; Kim, K. S.; Noh, D. Y.; Kim, K. S.; Chung, J. W. Control of the Plasmon in a Single Layer Graphene by Charge Doping. *Appl. Phys. Lett.* **2011**, *99*, 082110–082110.
55. Gass, M. H.; Bangert, U.; Bleloch, A. L.; Wang, P.; Nair, R. R.; Geim, A. K. Free-Standing Graphene at Atomic Resolution. *Nat. Nanotechnol.* **2008**, *3*, 676–681.
56. Fei, Z.; Rodin, A. S.; Andreev, G. O.; Bao, W.; McLeod, A. S.; Wagner, M.; Zhang, L. M.; *et al.* Gate-Tuning of Graphene Plasmons Revealed by Infrared Nano-Imaging. *Nature* **2012**, *487*, 82–85.
57. Kreibig, U.; Vollmer, M. *Optical Properties of Metal Clusters*; Springer-Verlag: New York, 1995.
58. Mie, G. BeitrAge Zur Optik TrUber Medien. *Ann. Phys.* **1908**, *25*, 377–445.
59. Berini, P. Plasmon-Polariton Waves Guided by Thin Lossy Metal Films of Finite Width: Bound Modes of Symmetric Structures. *Phys. Rev. B: Condens. Matter* **2000**, *61*, 10484.
60. Braun, J.; Gompf, B.; Kobiela, G.; Dressel, M. How Holes Can Obscure the View: Suppressed Transmission

through an Ultrathin Metal Film by a Subwavelength Hole Array. *Phys. Rev. Lett.* **2009**, *103*, 203901.
61. Dionne, J. A.; Sweatlock, L. A.; Atwater, H. A.; Polman, A. Planar Metal Plasmon Waveguides: Frequency-Dependent Dispersion, Propagation, Localization, and Loss Beyond the Free Electron Model. *Phys. Rev. B: Condens. Matter* **2005**, *72*, 075405.
62. Spevak, I. S.; Nikitin, A. Y.; Bezuglyi, E. V.; Levchenko, A.; Kats, A. V. Resonantly Suppressed Transmission and Anomalously Enhanced Light Absorption in Periodically Modulated Ultrathin Metal Films. *Phys. Rev. B: Condens. Matter* **2009**, *79*, 161406.
63. Ju, L.; Geng, B.; Horng, J.; Girit, C.; Martin, M.; Hao, Z.; Bechtel, H. A.; *et al.* Graphene Plasmonics for Tunable Terahertz Metamaterials. *Nat. Nanotechnol.* **2011**, *6*, 630–634.
64. Nikitin, A. Y.; Guinea, F.; Garcia-Vidal, F. J.; Martin-Moreno, L. Surface Plasmon Enhanced Absorption and Suppressed Transmission in Periodic Arrays of Graphene Ribbons. *Phys. Rev. B: Condens. Matter* **2012**, *85*, 081405.
65. Mikhailov, S. A.; Savostianova, N. A. Microwave Response of a Two-Dimensional Electron Stripe. *Phys. Rev. B: Condens. Matter* **2005**, *71*, 035320.
66. Jr, S. J. A.; Tsui, D. C.; Logan, R. A. Observation of the Two-Dimensional Plasmon in Silicon Inversion Layers. *Phys. Rev. Lett.* **1977**, *38*, 980–983.
67. Chen, J.; Badioli, M.; Alonso-Gonzlez, P.; Thongrattanasiri, S.; Huth, F.; Osmond, J.; Spasenović, M.; *et al.* Optical Nano-Imaging of Gate-Tunable Graphene Plasmons. *Nature* **2012**, *487*, 77–81.
68. Pohl, D. W.; Courjon, D. *Near Field Optics*; Kluwer Academic: Dordrecht, 1993; Vol. 2.
69. Zayats, A. V.; Smolyaninov, I. I.; Maradudin, A. A. Nano-Optics of Surface Plasmon Polaritons. *Phys. Rep.* **2005**, *408*, 131–314.
70. Kretschmann, E.; Raether, H. Radiative Decay of Non Radiative Surface Plasmons Excited by Light (Surface Plasma Waves Excitation by Light and Decay into Photons Applied to Nonradiative Modes). *Z. Naturforsch. A* **1968**, *23*, 2135.
71. Otto, A. Excitation of Nonradiative Surface Plasma Waves in Silver by the Method of Frustrated Total Reflection. *Z. Phys.* **1968**, *216*, 398–410.
72. Bludov, Y. V.; Ferreira, A.; Peres, N. M. R.; Vasilevskiy, M. I. A Primer on Surface Plasmon-Polaritons in Graphene. *Int. J. Mod. Phys. B* **2013**, *27*, No. 1341001.
73. Gao, W.; Shu, J.; Qiu, C.; Xu, Q. Excitation of Plasmonic Waves in Graphene by Guided-Mode Resonances. *ACS Nano* **2012**, *6*, 7806–7813.
74. Gao, W.; Shi, G.; Jin, Z.; Shu, J.; Zhang, Q.; Vajtai, R.; Ajayan, P. M.; Kono, J.; Xu, Q. Excitation and Active Control of Propagating Surface Plasmon Polaritons in Graphene. *Nano Lett.* **2013**, *13*, 36983702.
75. Schiefele, J.; Pedrs, J.; Sols, F.; Calle, F.; Guinea, F. Coupling Light into Graphene Plasmons through Surface Acoustic Waves. **2013**, arXiv:1309.0767.
76. Mooradian, A.; Wright, G. B. Observation of the Interaction of Plasmons with Longitudinal Optical Phonons in Gaas. *Phys. Rev. Lett.* **1966**, *16*, 999.
77. Fuchs, R.; Kliewer, K. L. Optical Modes of Vibration in an Ionic Crystal Slab. *Phys. Rev.* **1965**, *140*, A2076.
78. Matz, R.; Lth, H. Conduction-Band Surface Plasmons in the Electron-Energy-Loss Spectrum of Gaas (110). *Phys. Rev. Lett.* **1981**, *46*, 1045–1045.
79. Hillenbrand, R.; Taubner, T.; Keilmann, F. Phonon-Enhanced Light-Matter Interaction at the Nanometre Scale. *Nature* **2002**, *418*, 159–162.
80. Huber, A.; Ocelic, N.; Taubner, T.; Hillenbrand, R. Nanoscale Resolved Infrared Probing of Crystal Structure and of Plasmon-Phonon Coupling. *Nano Lett.* **2006**, *6*, 774–778.
81. Neubrech, F.; Pucci, A.; Cornelius, T. W.; Karim, S.; Garca-Etxarri, A.; Aizpurua, J. Resonant Plasmonic and Vibrational Coupling in a Tailored Nanoantenna for Infrared Detection. *Phys. Rev. Lett.* **2008**, *101*, 157403.
82. Fei, Z.; Andreev, G. O.; Bao, W.; Zhang, L. M.; McLeod, A. S.; Wang, C.; Srewart, M. K.; *et al.* Infrared Nanoscopy of Dirac Plasmons at the Graphene−$SiO_2$ Interface. *Nano Lett.* **2011**, *11*, 4701–4705.
83. Koch, R. J.; Seyller, T.; Schaefer, J. A. Strong Phonon-Plasmon Coupled Modes in the Graphene/Silicon Carbide Heterosystem. *Phys. Rev. B: Condens. Matter* **2010**, *82*, 201413.
84. Hwang, E. H.; Sensarma, R.; Sarma, S. D. Plasmon-Phonon Coupling in Graphene. *Phys. Rev. B: Condens. Matter* **2010**, *82*, 195406.
85. Low, T.; Perebeinos, V.; Kim, R.; Freitag, M.; Avouris, P. Cooling of Photoexcited Carriers in Graphene by Internal and Substrate Phonons. *Phys. Rev. B: Condens. Matter* **2012**, *86*, 045413.
86. Mikhailov, S. A. Radiative Decay of Collective Excitations in an Array of Quantum Dots. *Phys. Rev. B: Condens. Matter* **1996**, *54*, 10335.
87. Principi, A.; Vignale, G.; Carrega, M.; Polini, M. Impact of Disorder on Dirac Plasmon Losses. *Phys. Rev. B: Condens. Matter* **2013**, *88*, 121405.
88. Langer, T.; Baringhaus, J.; Pfnr, H.; Schumacher, H. W.; Tegenkamp, C. Plasmon Damping below the Landau Regime: The Role of Defects in Epitaxial Graphene. *New J. Phys.* **2010**, *12*, 033017.
89. Principi, A.; Vignale, G.; Carrega, M.; Polini, M. Intrinsic Lifetime of Dirac Plasmons in Graphene. **2013**, arXiv:1305.4666.
90. Zhu, W.; Low, T.; Perebeinos, V.; Bol, A. A.; Zhu, Y.; Yan, H.; Tersoff, J.; Avouris, P. Structure and Electronic Transport in Graphene Wrinkles. *Nano Lett.* **2012**, *12*, 3431–3436.
91. Low, T.; Perebeinos, V.; Tersoff, J.; Avouris, P. Deformation and Scattering in Graphene over Substrate Steps. *Phys. Rev. Lett.* **2012**, *108*, 096601.
92. Chen, J.-H.; Jang, C.; Xiao, S.; Ishigami, M.; Fuhrer, M. S. Intrinsic and Extrinsic Performance Limits of Graphene Devices on $SiO_2$. *Nat. Nanotechnol.* **2008**, *3*, 206–209.
93. Tassin, P.; Koschny, T.; Soukoulis, C. M. Graphene for Terahertz Applications. *Science* **2013**, *341*, 620–621.
94. Link, S.; El-Sayed, M. A. Spectral Properties and Relaxation Dynamics of Surface Plasmon Electronic Oscillations in Gold and Silver Nanodots and Nanorods. *J. Phys. Chem. B* **1999**, *103*, 8410–8426.
95. Yan, H.; Li, Z.; Li, X.; Zhu, W.; Avouris, P.; Xia, F. Infrared Spectroscopy of Tunable Dirac Terahertz Magneto-Plasmons in Graphene. *Nano Lett.* **2012**, *12*, 3766–3771.
96. Crassee, I.; Orlita, M.; Potemski, M.; Walter, A. L.; Ostler, M.; Seyller, T.; Gaponenko, I.; Chen, J.; Kuzmenko, A. B. Plasmons and Magnetoplasmons in Large Scale Monolayer Graphene. *Nano Lett.* **2012**, *12*, 2470.
97. Petkovic, I.; Williams, F. I. B.; Bennaceur, K.; Portier, F.; Roche, P.; Glattli, D. C. Carrier Drift Velocity and Edge Magnetoplasmons in Graphene. *Phys. Rev. Lett.* **2013**, *110*, 016801.
98. Echtermeyer, T. J.; Britnell, L.; Jasnos, P. K.; Lombardo, A.; Gorbachev, R. V.; Grigorenko, A. N.; Geim, A. K.; Ferrari, A. C.; Novoselov, K. S. Strong Plasmonic Enhancement of Photovoltage in Graphene. *Nat. Commun.* **2011**, *2*, 458.
99. Freitag, M.; Low, T.; Xia, F.; Avouris, P. Photoconductivity of Biased Graphene. *Nat. Photonics* **2012**, *7*, 53–59.
100. Yan, J.; Kim, M. H.; Elle, J. A.; Sushkov, A. B.; Jenkins, G. S.; Milchberg, H. M.; Fuhrer, M. S.; Drew, H. D. Dual-Gated Bilayer Graphene Hot-Electron Bolometer. *Nat. Nanotechnol.* **2012**, *7*, 472–478.
101. Xu, X.; Gabor, N. M.; Alden, J. S.; van der Zande, A. M.; McEuen, P. L. Photo-Thermoelectric Effect at a Graphene Interface Junction. *Nano Lett.* **2009**, *10*, 562–566.
102. Gabor, N. M.; Song, J. C.; Ma, Q.; Nair, N. L.; Taychatanapat, T.; Watanabe, K.; Taniguchi, T.; Levitov, L. S.; Jarillo-Herrero, P. Hot CarrierAssisted Intrinsic Photoresponse in Graphene. *Science* **2011**, *334*, 648–652.
103. Mueller, T.; Xia, F.; Freitag, M.; Tsang, J.; Avouris, P. Role of Contacts in Graphene Transistors: A Scanning Photocurrent Study. *Phys. Rev. B: Condens. Matter* **2009**, *79*, 245430.

104. Engel, M.; Steiner, M.; Lombardo, A.; Ferrari, A. C.; Lhneysen, H. V.; Avouris, P.; Krupke, R. LightMatter Interaction in a Microcavity-Controlled Graphene Transistor. *Nat. Commun.* **2012**, *3*, 906.
105. Furchi, M.; Urich, A.; Pospischil, A.; Lilley, G.; Unterrainer, K.; Detz, H.; Klang, P.; *et al.* Microcavity-Integrated Graphene Photodetector. *Nano Lett.* **2012**, *12*, 2773–2777.
106. Gan, X.; Shiue, R.-J.; Gao, Y.; Meric, I.; Heinz, T. F.; Shepard, K.; Hone, J.; Assefa, S.; Englund, D. Chip-Integrated Ultrafast Graphene Photodetector with High Responsivity. *Nat. Photonics* **2013**, 883–887.
107. Pospischil, A.; Humer, M.; Furchi, M. M.; Bachmann, D.; Guider, R.; Fromherz, T.; Mueller, T. CMOS-Compatible Graphene Photodetector Covering All Optical Communication Bands. *Nat. Photonics* **2013**, *7*, 892–896.
108. Liu, Y.; Cheng, R.; Liao, L.; Zhou, H.; Bai, J.; Liu, G.; Liu, L.; Huang, Y.; Duan, X. Plasmon Resonance Enhanced Multicolour Photodetection by Graphene. *Nat. Commun.* **2011**, *2*, 579.
109. Rogalski, A. *Infrared Detectors*; CRC Press: Boca Raton, FL, 2010.
110. Vakil, A.; Engheta, N. Transformation Optics Using Graphene. *Science* **2011**, *332*, 1291–1294.
111. Chen, H.-T.; Padilla, W. J.; Zide, J. M.; Gossard, A. C.; Taylor, A. J.; Averitt, R. D. Active Terahertz Metamaterial Devices. *Nature* **2006**, *444*, 597–600.
112. Chen, H.-T.; Padilla, W. J.; Cich, M. J.; Azad, A. K.; Averitt, R. D.; Taylor, A. J. A Metamaterial Solid-State Terahertz Phase Modulator. *Nat. Photonics* **2009**, *3*, 148–151.
113. Landy, N. I.; Sajuyigbe, S.; Mock, J. J.; Smith, D. R.; Padilla, W. J. Perfect Metamaterial Absorber. *Phys. Rev. Lett.* **2008**, *100*, 207402.
114. Hwang, E. H.; Sarma, S. D. Plasmon Modes of Spatially Separated Double-Layer Graphene. *Phys. Rev. B: Condens. Matter* **2009**, *80*, 205405.
115. Lee, S. H.; Choi, M.; Kim, T.-T.; Lee, S.; Liu, M.; Yin, X.; Choi, H. K.; *et al.* Switching Terahertz Waves with Gate-Controlled Active Graphene Metamaterials. *Nat. Mater.* **2012**, *11*, 936–941.
116. Carrasco, E.; Tamagnone, M.; Perruisseau-Carrier, J. Tunable Graphene Reflective Cells for Thz Reflectarrays and Generalized Law of Reflection. *Appl. Phys. Lett.* **2013**, *102*, 104103–104103.
117. Huang, J. *Reflectarray Antenna*; John Wiley and Sons, Inc.: Hoboken, NJ, 2008.
118. Hum, S. V.; Perruisseau-Carrier, J. Reconfigurable Reflectarrays and Array Lenses for Dynamic Antenna Beam Control: A Review. **2013**, arXiv:1308.4593.
119. Thongrattanasiri, S.; Koppens, F. H.; de Abajo, F. Complete Optical Absorption in Periodically Patterned Graphene. *Phys. Rev. Lett.* **2012**, *108*, 047401.
120. Chen, P.-Y.; Alu, A. Atomically Thin Surface Cloak Using Graphene Monolayers. *ACS Nano* **2011**, *5*, 5855–5863.
121. Iorsh, I. V.; Mukhin, I. S.; Shadrivov, I. V.; Belov, P. A.; Kivshar, Y. S. Hyperbolic Metamaterials Based on Multilayer Graphene Structures. *Phys. Rev. B: Condens. Matter* **2013**, *87*, 075416.
122. Andryieuski, A.; Lavrinenko, A. V.; Chigrin, D. N. Graphene Hyperlens for Terahertz Radiation. *Phys. Rev. B: Condens. Matter* **2012**, *86*, 121108.
123. Adato, R.; Yanik, A. A.; Amsden, J. J.; Kaplan, D. L.; Omenetto, F. G.; Hong, M. K.; Erramilli, S.; Altug, H. Ultra-Sensitive Vibrational Spectroscopy of Protein Monolayers with Plasmonic Nanoantenna Arrays. *Proc. Natl. Acad. Sci. U.S.A.* **2009**, *106*, 19227–19232.
124. Liu, F.; Cubukcu, E. Tunable Omnidirectional Strong Light-Matter Interactions Mediated by Graphene Surface Plasmons. *Phys. Rev. B: Condens. Matter* **2013**, *88*, 115439.
125. Colthup, N. B.; Daly, L. H.; Wiberley, S. E. *Introduction to Infrared and Raman Spectroscopy*; Academic Press: Boston, MA,1990.
126. Ponath, H.-E.; Stegeman, G. I. *Nonlinear Surface Electromagnetic Phenomena*; Elsevier: New York, 1991.
127. Xu, G.; Tazawa, M.; Jin, P.; Nakao, S.; Yoshimura, K. Wavelength Tuning of Surface Plasmon Resonance Using Dielectric Layers on Silver Island Films. *Appl. Phys. Lett.* **2003**, *82*, 3811–3813.
128. Neubrech, F.; Kolb, T.; Lovrincic, R.; Fahsold, G.; Pucci, A.; Aizpurua, J.; Cornelius, T. W.; Toimil-Molares, M. E.; Neumann, R.; Karim, S. Resonances of Individual Metal Nanowires in the Infrared. *Appl. Phys. Lett.* **2006**, *89*, 253104.
129. Novotny, L. Effective Wavelength Scaling for Optical Antennas. *Phys. Rev. Lett.* **2007**, *98*, 266802.
130. Novoselov, K. S.; McCann, E.; Morozov, S. V.; Falko, V. I.; Katsnelson, M. I.; Zeitler, U.; Jiang, D.; Schedin, F.; Geim, A. K. Unconventional Quantum Hall Effect and Berrys Phase of 2 in Bilayer Graphene. *Nat. Phys.* **2006**, *2*, 177.
131. Ohta, T.; Bostwick, A.; Seyller, T.; Horn, K.; Rotenberg, E. Controlling the Electronic Structure of Bilayer Graphene. *Science* **2006**, *313*, 951.
132. McCann, E. Asymmetry Gap in the Electronic Band Structure of Bilayer Graphene. *Phys. Rev. B: Condens. Matter* **2006**, *74*, No. 161403(R).
133. Yan, J.; Villarson, T.; Henriksen, E. A.; Kim, P.; Pinczuk, A. Optical Phonon Mixing in Bilayer Graphene with a Broken Inversion Symmetry. *Phys. Rev. B: Condens. Matter* **2009**, *80*, 241417.
134. Tang, T.-T.; Zhang, Y.; Park, C.-H.; Geng, B.; Girit, C.; Hao, Z.; Martin, M. C.; *et al.* A Tunable PhononExciton Fano System in Bilayer Graphene. *Nat. Nanotechnol.* **2009**, *5*, 32–36.
135. Kuzmenko, A. B.; Benfatto, L.; Cappelluti, E.; Crassee, I.; Marel, D. V. D.; Blake, P.; Novoselov, K. S.; Geim, A. K. Gate Tunable Infrared Phonon Anomalies in Bilayer Graphene. *Phys. Rev. Lett.* **2009**, *103*, 116804.
136. Yan, H.; Low, T.; Guinea, F.; Xia, F.; Avouris, P. Tunable Phonon-Induced Transparency in Bilayer Graphene Nanoribbons. **2013**, arXiv:1310.4394.
137. Cappelluti, E.; Benfatto, L.; Kuzmenko, A. B. Phonon Switching and Combined Fano-Rice Effect in Optical Spectra of Bilayer Graphene. *Phys. Rev. B: Condens. Matter* **2010**, *82*, 041402.
138. Low, T.; Guinea, F.; Yan, H.; Xia, F.; Avouris, P. Novel Mid-Infrared Plasmonic Effects in Bilayer Graphene. **2013**, arXiv:1310.4693.
139. Aroca, R. F.; Ross, D. J.; Domingo, C. Surface-Enhanced Infrared Spectroscopy. *Appl. Spectrosc.* **2004**, *58*, 324A–338A.
140. Thongrattanasiri, S.; de Abajo, F. J. G. Optical Field Enhancement by Strong Plasmon Interaction in Graphene Nanostructures. *Phys. Rev. Lett.* **2013**, *110*, 187401.
141. Novoselov, K. S.; Jiang, D.; Schedin, F.; Booth, T. J.; Khotkevich, V. V.; Morozov, S. V.; Geim, A. K. Two-Dimensional Atomic Crystals. *Proc. Natl. Acad. Sci. U.S.A.* **2005**, *102*, 10451–10453.
142. Wang, Q. H.; Kalantar-Zadeh, K.; Kis, A.; Coleman, J. N.; Strano, M. S. Electronics and Optoelectronics of Two-Dimensional Transition Metal Dichalcogenides. *Nat. Nanotechnol.* **2012**, *7*, 699–712.
143. Chhowalla, M.; Shin, H. S.; Eda, G.; Li, L.-J.; Loh, K. P.; Zhang, H. The Chemistry of Two-Dimensional Layered Transition Metal Dichalcogenide Nanosheets. *Nat. Chem.* **2013**, *5*, 263–275.
144. Mas-Balleste, R.; Gomez-Navarro, C.; Gomez-Herrero, J.; Zamora, F. 2D Materials: To Graphene and Beyond. *Nanoscale* **2011**, *3*, 20–30.
145. Britnell, L.; Ribeiro, R. M.; Eckmann, A.; Jalil, R.; Belle, B. D.; Mishchenko, A.; Kim, Y.-J.; *et al.* Strong Light-Matter Interactions in Heterostructures of Atomically Thin Films. *Science* **2013**, *340*, 1311–1314.
146. Zhang, H.; Liu, C.-X.; Qi, X.-L.; Dai, X.; Fang, Z.; Zhang, S.-C. Topological Insulators in Bi2se3, Bi2te3 and Sb2te3 with a Single Dirac Cone on the Surface. *Nat. Phys.* **2009**, *5*, 438–442.
147. Neto, A. C. Charge Density Wave, Superconductivity, and Anomalous Metallic Behavior in 2D Transition Metal Dichalcogenides. *Phys. Rev. Lett.* **2001**, *86*, 4382.
148. Wilson, J. A.; Salvo, F. J. D.; Mahajan, S. Charge-Density Waves and Superlattices in the Metallic Layered

Transition Metal Dichalcogenides. *Adv. Phys.* **1975**, *24*, 117–201.
149. Mak, K. F.; He, K.; Shan, J.; Heinz, T. F. Control of Valley Polarization in Monolayer $MoS_2$ by Optical Helicity. *Nat. Nanotechnol.* **2012**, *7*, 494–498.
150. Zeng, H.; Dai, J.; Yao, W.; Xiao, D.; Cui, X. Valley Polarization in Mos2Monolayers by Optical Pumping. *Nat. Nanotechnol.* **2012**, *7*, 490–493.